TURBULENT DISSIPATION RATE MEASUREMENTS IN PLANE AND AXISYMMETRIC WAKE FLOWS

by

Toralf C. SCHENCK, and Jovan R. JOVANOVIĆ

Original scientific paper
UDC: 532.517.4/.55
BIBLID: 0354–9836, *5* (2001), 1, 75–100

All first-order spatial derivatives of the turbulent velocity fluctuations were measured using a pair of X hot-wire probes. Measurements were performed in the self-preserving region of a turbulent plane wake downstream of a cylinder and in an axisymmetric wake behind the sphere. Good spatial resolution of the measurements was ensured by choosing small values for the cylinder/sphere diameter and a low flow speed. Errors due to the finite hot-wire length and the wire and probe separation were analysed using Wyngaard's correction method. The derived corrections were verified experimentally. The measuring technique and the experimental results were systematically checked and compared with the results available in the literature. The assumptions of local isotropy and local axisymmetry were examined. Both investigated flows deviate only moderately from local isotropy and local axisymmetry. Support for the measured results is provided by plotting the data on an anisotropy invariant map. The budgets of the turbulent kinetic energy were computed from the measured data. In contrast to the results obtained in the plane wake, where the pressure transport is nearly negligible, in the axisymmetric wake it was found to play an important role and closely follows the estimate made by Lumley, $\overline{u_i p}/\rho \approx -0.2\overline{q^2 u_i}$.

INTRODUCTION

The dissipation correlations $\epsilon_{ij} = \nu \overline{\frac{\partial u_i}{\partial x_k}\frac{\partial u_j}{\partial x_k}}$ play an important role in turbulence modelling, since these represent a sink term in the Reynolds stress equations. The trace of the dissipation tensor ϵ[1] appears in nearly all turbulent models. Modelling of the dissipation rate correlations is the weakest part of the turbulence closures

[1] ϵ and the total average turbulent dissipation rate $\bar{\epsilon}$ are related as follows:

$$\bar{\epsilon} = \nu \overline{\frac{\partial u_i}{\partial x_k}\left(\frac{\partial u_i}{\partial x_k} + \frac{\partial u_k}{\partial x_i}\right)} = \nu \overline{\frac{\partial u_i}{\partial x_k}\frac{\partial u_i}{\partial x_k}} + \nu \frac{\partial^2 \overline{u_i u_k}}{\partial x_i \partial x_k}.$$

The second term on the right-hand side is negligible in the wake flows under consideration

since the dynamics of ϵ_{ij} are extremely complicated. Often they are modelled assuming local isotropy, as proposed by Kolmogorov [1]. An exception is the near-wall region where empirical wall functions are used to recast the data. One of many difficulties also originates from an insufficient amount of numerical or experimental data that can be of some use for direct validation of the closure assumptions used to construct a transport equation for the dissipation rate. Although direct numerical simulations have been available for almost 20 years, only very few data sets contain useful information about terms in the transport equation of the turbulent dissipation rate. In this respect, two-point statistics would be extremely useful but are not available. Experimental data are also rare, since measurements of the relevant terms are very difficult or even impossible.

The first dissipation measurements were made by Simmons and Salter [2] using hot-wire probes together with Taylor's frozen flow hypothesis and assuming isotropy in the dissipation range. In a similar way, the turbulent dissipation rate was measured in a turbulent jet by Corrsin [3] and Corrsin and Uberoi [4] and in a plane wake by Townsend [5,6]. Townsend measured statistics of the streamwise derivatives which provided support for the applicability of the assumption of local isotropy. Laufer [7] and Klebanoff [8] measured five of the nine terms of the turbulent dissipation rate in a turbulent pipe flow and in a flat plate boundary layer, respectively. For the determination of the remaining terms they applied isotropic relationships. All three components of the temperature dissipation rate were measured in a turbulent wake flow by Uberoi and Freymuth [9] and Antonia and Browne [10]. The same quantities were also measured by Tavoularis and Corrsin [11,12] in a homogeneous shear flow and by Krishnamoorthy and Antonia [13] in a turbulent boundary layer.

Using a pair of X hot-wire probes, Browne *et al.* [14] measured all nine terms of the turbulent dissipation rate. Instead of ϵ the authors determined the dissipation from $\overline{\epsilon}$ and assumed local isotropy for the three remaining terms. George and Hussein [15] and Hussein *et al.* [16] used the flying hot-wire technique for measuring five of the nine dissipation terms in a round jet at high Reynolds numbers. A similar experiment was performed by Hussein [17], who measured seven of nine terms of ϵ in a plane jet. The results obtained in this study showed that local axisymmetry is a better approximation than local isotropy.

Ye [18] measured all nine terms of the turbulent dissipation rate and three components of the dissipation tensor in a turbulent plane wake using the same technique as Browne *et al.* [14]. The measurements described in this paper are an extension of the work of Browne *et al.* [14] and Ye [18]. Instead of a fixed X hot-wire configuration, two probes with variable separation were employed, allowing precise relative alignment and the possibility of performing various test measurements. The paper focuses mainly on experimental aspects such as corrections and accuracy tests. At the end of the paper we provide distributions of the individual terms involved in the transport equation for turbulent kinetic energy. A detailed investigation and

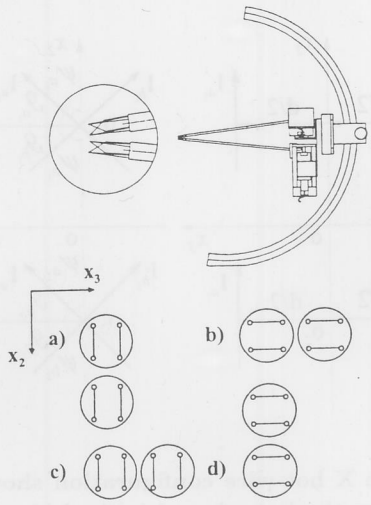

Figure 1. Different configurations of X hot-wire probes employed for measurements of the instantaneous velocity derivatives. (a) $u_{1,1}$, $u_{1,2}$, $u_{2,1}$, $u_{2,2}$; (b) $u_{1,1}$, $u_{1,3}$, $u_{3,1}$, $u_{3,3}$; (c) $u_{1,1}$, $u_{1,3}$, $u_{2,1}$, $u_{2,3}$; (d) $u_{1,1}$, $u_{1,2}$, $u_{3,1}$, $u_{3,2}$

validation turbulence closure of the dissipation correlations using the experimental data will be the subject of a future paper.

EXPERIMENTAL TECHNIQUE FOR MEASURING VELOCITY DERIVATIVES

Spatial derivatives of the fluctuating velocities can be obtained experimentally by measuring the velocity difference at two closely spaced points, $u_{i,j} = \partial u_i/\partial x_j \approx \Delta u_i/\Delta x_j$. This technique, known as the finite-difference method, was used in several studies by Browne *et al.* [14], Ye [18], and Zhu and Antonia [19]. Using a pair of X hot-wire probes of different configurations all nine components of the turbulent dissipation rate ϵ can be measured, as shown in Fig. 1, which provide details of a wind-tunnel arrangement of two closely separated X hot-wire probes used for the velocity derivative measurements. The sketch shows probe holders, the device used for calibration of hot wires at known yaw angles in the wind tunnel (top) and different configurations of X hot-wire probes (bottom). Here, the coordinates x_2 and x_3 lie in the plane perperdicular to the flow which is along the x_1 direction.

In the analysis of the data measured by different hot-wire configurations shown in Fig. 1, it was necessary to account for the spatial filtering arising from the finite length (l) of the hot wires and also for the wire (d) and probe (s) separation. For this purpose, the correction procedure suggested by Wyngaard [20,21], and extended by

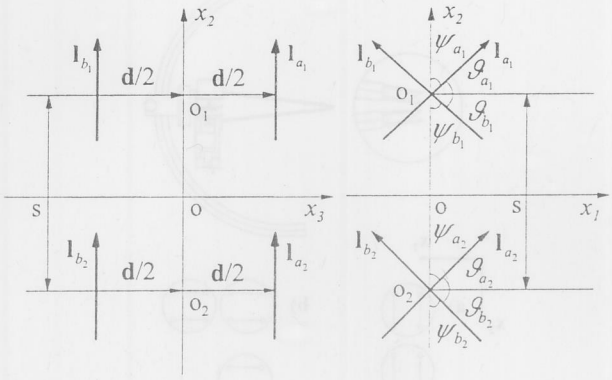

Figure 2. Schematic of the X hot-wire configuration shown in Fig. 1(a). Here d is the distance between the hot wires, l is the hot-wire length, s is the distance between two probes and ψ is the effective wire angle

Zhu and Antonia [19], was applied. Here we provide a brief summary of the correction method used to evaluate the data.

Assuming that turbulence is homogeneous, the derivative $\overline{(\partial u_1/\partial x_2)^2}$ can be expressed by

$$\overline{\left(\frac{\partial u_1}{\partial x_2}\right)^2} = \int_{-\infty}^{\infty}\int_{-\infty}^{\infty}\int_{-\infty}^{\infty} k_2^2\,\phi_{11}(\mathbf{k})dk_1dk_2dk_3 \tag{1}$$

where $\mathbf{k}$ is the wavenumber vector, $\mathbf{k} = (k_1, k_2, k_3)$, and ϕ_{11} is the energy spectral tensor. The measured velocity derivative spectrum $\phi^m_{u_{1,2}}$ for the hot-wire configuration (a) shown in Figs. 1 and 2 can be represented by

$$\begin{aligned}\phi^m_{u_{1,2}}(\mathbf{k}) &= 1/s^2\sin^2(k_2s/2)\{\phi_{11}[(X_a^2+X_b^2)+2X_aX_b\cos(k_3d)]\\ &+ 2\cot\vartheta\,\phi_{12}(X_b^2-X_a^2)\\ &+ \cot^2\vartheta\,\phi_{22}[(X_a^2+X_b^2)-2X_aX_b\cos(k_3d)]\}\end{aligned} \tag{2}$$

where $X_a = \sin(\mathbf{kl}_a)/(\mathbf{kl}_a)$ originate from the filtering effect due to the finite length of the hot-wire (Zhu and Antonia, [19]). The use of the above equation assumes homogeneity of turbulence, uniformity of the mean velocity field across the hot-wire and small turbulence intensity. With eqs. (1) and (2) one can estimate the ratio

$$r_{12} = \frac{\overline{(\partial u_1/\partial x_2)^2}^m}{\overline{(\partial u_1/\partial x_2)^2}} = \frac{\int\int\int_{-\infty}^{\infty}\phi^m_{u_{1,2}}(\mathbf{k})dk_1dk_2dk_3}{\int\int\int_{-\infty}^{\infty}k_2^2\,\phi_{11}(\mathbf{k})dk_1dk_2dk_3} \tag{3}$$

by integrating eq. (3) numerically with the assumed isotropic form for ϕ_{ij}:

$$\phi_{ij}(\mathbf{k}) = \frac{E(k)}{4\pi k^4}\left(k^2\delta_{ij} - k_ik_j\right) \tag{4}$$

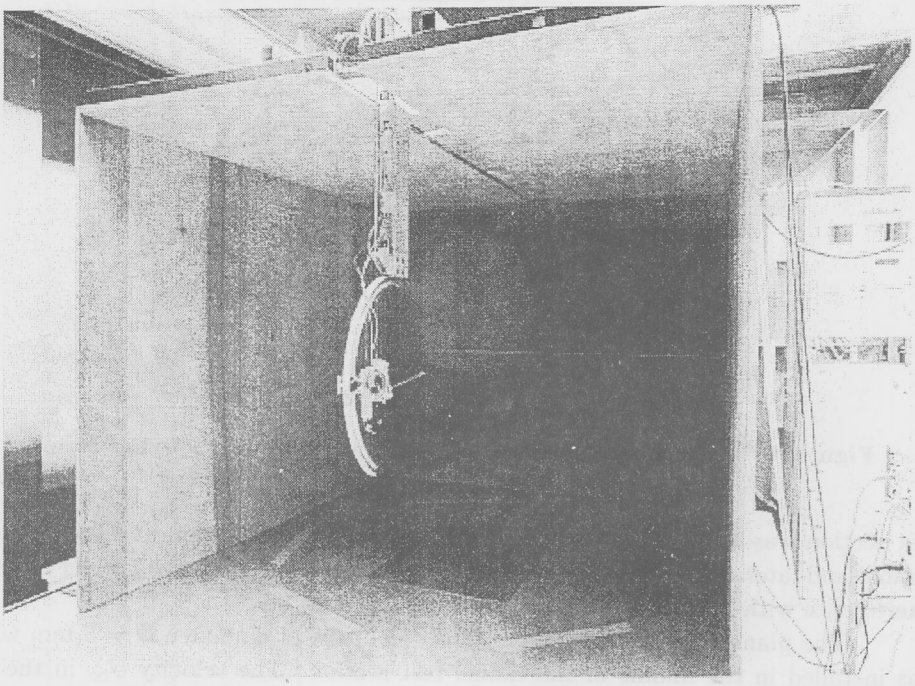

Figure 3. The test section of a wind tunnel at the Lehrstuhl für Strömungsmechanik Erlangen

where $E(k)$ is the three-dimensional energy spectrum. In the same way, corrections for all other gradients can be defined.

Zhu and Antonia [19] used $E(k)$ from the DNS data for a turbulent channel flow to evaluate the data. In the present study the form of $E(k)$ suggested by Pao [22] was used to estimate the influence of the wire length and the wire and probe separation on measured statistics of the velocity derivatives. Because of the implied isotropy assumption involved in approximation of the energy spectrum, $E(k)$ corrections must be verified before they can be applied.

Wind tunnel setup and instrumentation

The experiments were carried out in the closed test section of a return-type wind tunnel at the Lehrstuhl für Strömungsmechanik, Erlangen (see Fig. 3). Its test section is 1.87 m wide, 1.40 m high and 2.0 m long. The flow uniformity in the wind tunnel and two-dimensionality of the plane wake were systematically investigated before performing the measurements. The free stream turbulence level in the empty

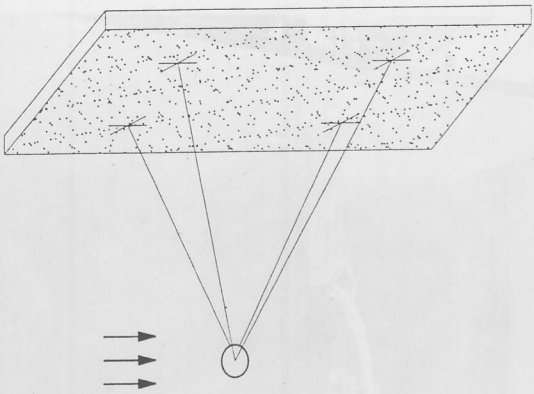

Figure 4. Experimental arrangement of a sphere in the wind tunnel

test section was approximately 0.07% in the streamwise direction and 0.04% in the normal and lateral directions. Since the free stream turbulence level was very low, no interference with the wake turbulence was expected.

The plane wake was generated by a steel tube of diameter $D = 3$ mm which was installed in the middle of the tunnel test section. The velocity U_∞ in the free stream was 6.6 m/s, corresponding to a Reynolds number based on the cylinder diameter of $R_D = 1340$. For generating the axisymmetric wake a sphere of diameter $D = 16$ mm was suspended using four thin wires (see Fig. 4). In order to avoid vortex shedding from the suspending wires, their diameter was only 50 μm. With a free stream velocity of 6.1 m/s the wire Reynolds number was 20, which is well below $Re_{crit} \approx 50$. The Reynolds number based on the sphere diameter was 6550.

The axisymmetry of the mean flow field was measured using a single hot-wire probe. Figure 5 shows distributions of turbulence intensity, skewness and flatness factors of the streamwise velocity component. Data from the contour plots shown in this figure display small radial asymmetries in the narrow region of the upper part of the wake which originate from disturbances caused by the suspending wires. Detailed profiles of mean velocity and turbulence quantities taken by horisontal and vertical traverses across the wake showed very small deviations and nearly perfect symmetry in the measured data (Schenck, [23]). It was decided, therefore, that data obtained from vertical traverses are good represntatives to quantify turbulence in the axisymmetric wake flow.

Detailed experimental investigations reported here were performed in the self-preserving region: 400 diameters downstream from the circular cylinder and 75 diameters behind the sphere. The self-similarity in the wake was checked by comparing mean velocity profiles, second- and third-order moments and statistics of the longitudinal gradient of the fluctuating u_1 velocity component taken at different streamwise

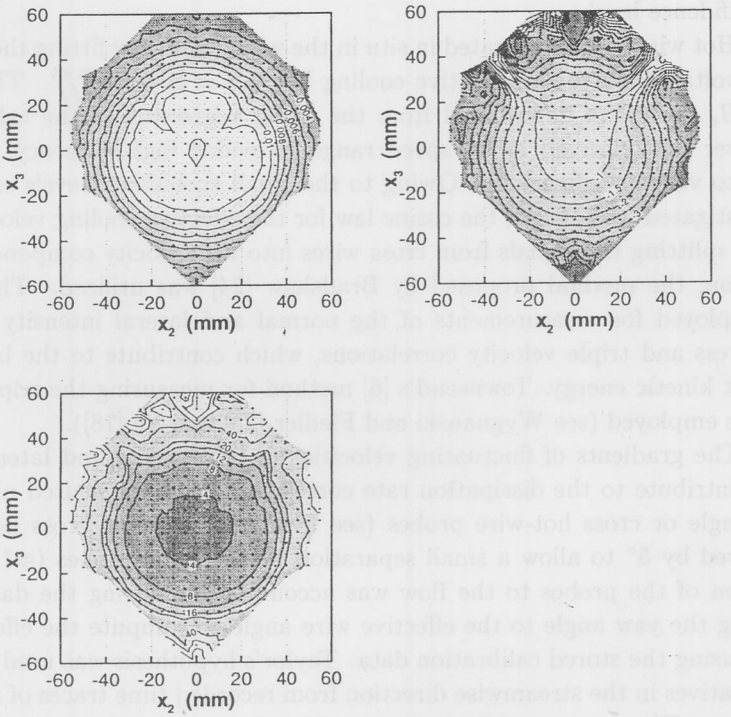

Figure 5. Contour plots of relative turbulence intensity u_1'/U_1 (top left), the skewness factor (top right) and the flatness factor (bottom) of the streamwise velocity component in the axisymmetric wake at $x_1/D = 101$

locations.

All measurements were made using standard DANTEC hot-wire probes operated with Dantec StreamLine constant temperature anemometers at an overheat ratio of 0.6. The output signals from the anemometers were passed through back-up amplifiers, low-pass filtered and then digitized and stored on a PC for further processing. For measurements of the mean velocity and turbulence intensities, single and X hot-wire probes (DANTEC 55P11 and 55P61 [2]) were used.

To ensure the statistical independence of the sampled data, the integral time-scale was measured from the autocorrelation function at various positions across the wake. This information was used to set the sampling interval to about two integral time-scales of the flow. The sample size at each measuring point was 25000 data taken at rate of 250 Hz. This sample size corresponds to a sampling error of 0.03% for the

[2]The hot-wire probes employed were made from Pt-plated tungsten wire, diameter 5 μm, length $l = 1.16 \pm 0.02$ mm and the separation between the wires was $d = 0.4 \pm 0.05$ mm

mean velocity and 2.3% for the second-order moments calculated on the basis of a 99% confidence level.

Hot wires were calibrated in situ in the wind tunnel by fitting the anemometer output voltage (E) to the effective cooling law $E^2 = A + BU_{eff}^{0.45}$. The coefficients A and B, that were determined from the linear regression of the calibration data taken over the relatively small speed range, provided high accuracy (0.2%) of the voltage to velocity conversion. Owing to the small turbulence levels encountered in the investigated wake flows, the cosine law for the effective cooling velocity U_{eff} was used for splitting the signals from cross wires into the velocity components. For yaw calibration, the method proposed by Bradshaw [24] was utilized. The cross wires were employed for measurements of the normal and lateral intensity components, shear stress and triple velocity correlations, which contribute to the balance of the turbulent kinetic energy. Townsend's [6] method for measuring the triple correlation $\overline{u_3^2 u_2}$ was employed (see Wygnanski and Fiedler [25] and Ye [18]).

The gradients of fluctuating velocities in the normal and lateral directions, which contribute to the dissipation rate correlations, were measured using a pair of either single or cross hot-wire probes (see Fig. 6). The two cross hot wires were each yawed by 5° to allow a small separation between the probes (≈1.6 mm). The inclination of the probes to the flow was accounted for during the data processing by adding the yaw angle to the effective wire angle to compute the effective cooling velocity using the stored calibration data. Taylor's hypothesis was used to determine the derivatives in the streamwise direction from recorded time traces of the measured fluctuations. The outputs of the hot-wire anemometers were first low-pass filtered at 5 kHz and then digitized at a sampling frequency f_S of 12 kHz. Prior to computing time derivatives, the data were additionally digitally low-pass filtered at the Kolmogorov frequency $f_k = U_1/2\pi L_k$ [$L_k = (\nu^3/\epsilon)^{1/4}$] using the NERD filter routines described by Kaiser and Reed [26]. The derivatives were then evaluated using $\Delta t = 2/f_S$ and subsequently corrected for the effects of finite hot-wire length, probe and wire separation.

EXPERIMENTAL RESULTS

Mean flow field

In order to ensure high reliability of the measured data, a number of qualifying tests were made. Several profiles of $u_1' = \sqrt{\overline{u_1^2}}$, u_2', u_3' were compared to check the repeatability of the measurements . For the plane wake flow most of the measured profiles are shown in Fig. 7. This figure shows complete profiles, *i. e.* both sides of the wake, and includes the data measured by all hot-wire configurations shown in Fig. 1. Note that for measurements of the instantaneous velocity derivatives it is important that both probes give nearly identical responses. The deviations between the individual curves are within a few percent and the agreement between single and

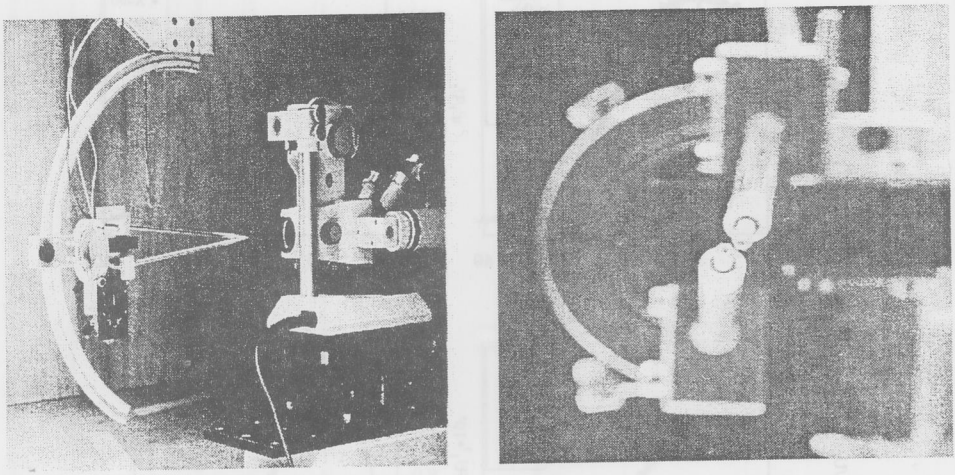

Figure 6. Photograph of the hot-wire mounting and the microscope for probe positioning in the wind tunnel (left). Enlarged front view of the hot-wire probes (right)

cross-wire measurements is seen to be very good. The data for the axisymmetric wake (not presented here) show nearly the same degree of agreement.

An additional check of the measured data can be made from the mean momentum equation. For the two-dimensional small-deficit wake this equation is

$$U_\infty \frac{\partial U_1}{\partial x_1} + \frac{\partial \overline{u_1 u_2}}{\partial x_2} = 0 \tag{5}$$

which can be rearranged in the form

$$\frac{\overline{u_1 u_2}}{U_S^2} = -\frac{A_L}{2A_U}\,\eta f \tag{6}$$

where A_L and A_U are the similarity constants. These can be expressed as

$$\frac{U_S}{U_\infty} = A_U \left(\frac{x_1 - x_{1,0}}{D}\right)^{-1/2}, \quad \frac{L}{D} = A_L \left(\frac{x_1 - x_{1,0}}{D}\right)^{1/2} \tag{7}$$

where U_S is the centerline mean-velocity defect, which measures the difference between the free stream and local mean velocities, $x_{1,0}$ is the virtual flow origin, η is the non-dimensional normal coordinate $\eta = x_2/L$, L is the half-width of the wake (where $U_S = 0.5$) and $f(\eta)$ is the normalized mean velocity distribution $f(\eta) = (U_\infty - U_1)/U_S$. Figure 8 shows the comparison between the measured data and values computed from eq. (6). At the position of maximum shear stress the deviation is about 10% and

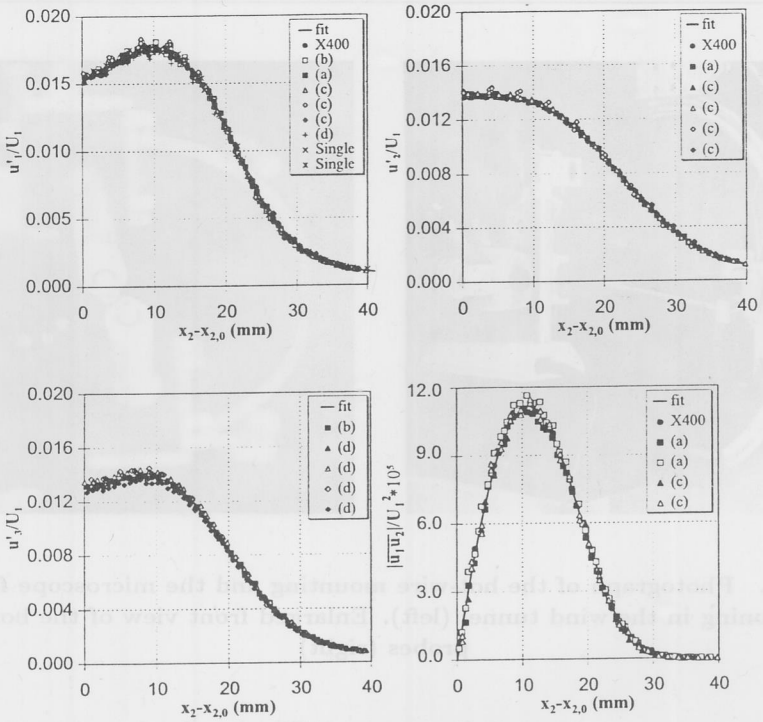

Figure 7. Comparisons of the intensity and shear stress distributions across the plane wake measured using single wire (denoted Single), cross wire (denoted X400) and configurations (a), (b), (c) and (d) shown in Fig. 1. Displayed data includes both side of the wake which cannot be distinguished owing to perfect symmetry of the flow

originates from uncertainties in the determination of the similarity constants involved in eq. (7), which were obtained by fitting the measured data at different streamwise positions in the wake (see Schenck, [23]). In the case of the axisymmetric wake the maximum deviation between the measured and calculated shear stress was 8%.

The measured mean velocity profiles were used to compute the momentum thickness:

$$\theta = \int_{-\infty}^{\infty} \frac{U_1}{U_\infty}\left(1 - \frac{U_1}{U_\infty}\right) dx_2 \tag{8}$$

which must be constant. Figure 8 (right) shows the computed values of θ at different locations behind the cylinder. The average value $\theta = 1.42 \pm 0.02$ mm corresponds to a drag coefficient $c_D = 2\theta/D$ of 0.95, which is identical with the result obtained by Wygnanski *et al.* [27] and is close to the value suggested in the literature (see Hoerner, [28]). The value of drag inferred from the measurements in the wake behind

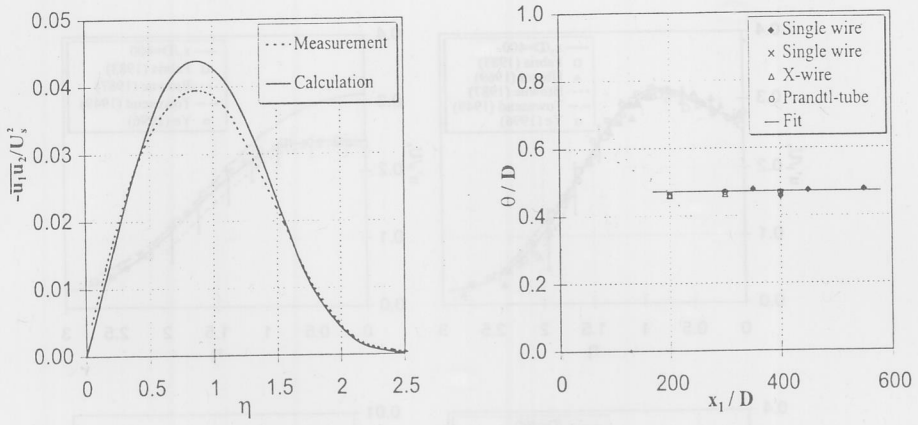

Figure 8. Normalized distributions of measured and calculated shear stress (left). Momentum thickness in the plane wake computed at different locations behind the cylinder (right)

the sphere, $c_D = 0.42$, is in good agreement with the data from the literature (Hoerner [28], $c_D = 0.42$; Schlichting and Gersten [29], $c_D = 0.40$).

The measured data were also compared with the results available from other studies reported in the literature. Since the shape of the self-similar profiles depends on the initial conditions, as shown by Wygnanski *et al.* [27], only the data from wake flows behind circular cylinders from Townsend [6], Fabris [30], Aronson and Löfdahl [31], Browne *et al.* [14], Uberoi and Freymuth [32] and Ye [18] were used for comparisons. However, only in the studies reported by Fabris [30] and Ye [18] were all stresses directly measured. Figure 9 shows comparisons of the turbulence intensities and the shear stress in the plane wake. The data from Browne *et al.* [14] are shown with error bars which indicate the maximum deviations between their data sets. The agreement is seen to be good, in particular with the data of Fabris [30] and Ye [18]. The source of the deviations of the present data from those measured by Townsend [6] could not be found. An attempt to apply the extended similarity theory proposed by George [33] was not successful and the data emerging from this analysis are not shown here.

Statistics of the velocity derivatives

In order to test the validity of the corrections discussed in the previous section, measurements with variable separation between hot-wire probes were performed. The derivatives in the streamwise direction were computed from the recorded time traces using the Taylor hypothesis. Figure 10 shows the measured and corrected derivatives

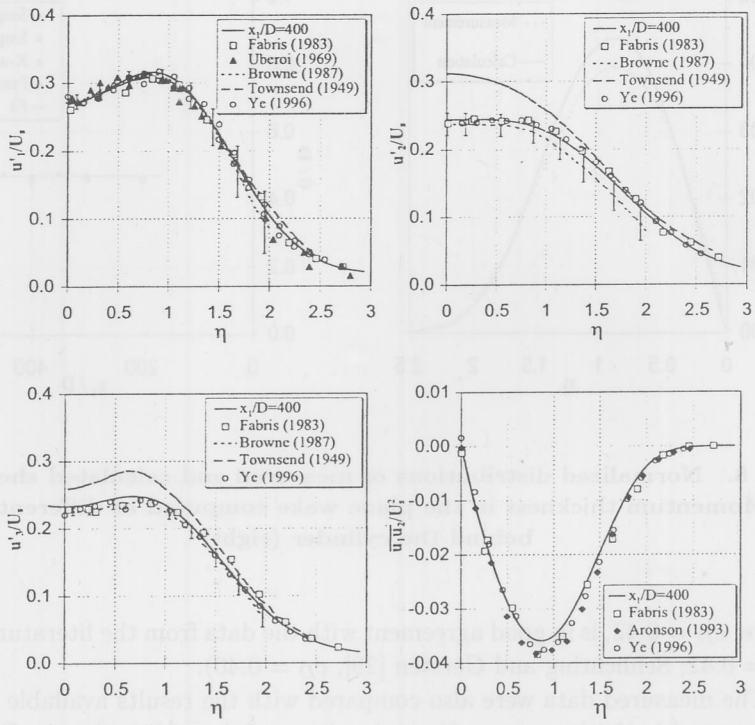

Figure 9. Comparisons of the measured intensity components and shear stress across the plane wake with the data available in the literature

$u'_{1,1} = \sqrt{\overline{(\partial u_1/\partial x_1)^2}}$, $u'_{3,1}$ and $u'_{1,3}$ as a function of the separation distance between the probes normalized by the Kolmogorov microscale L_k [3]. The displayed data correspond to the centerline region and the outer part of the wake and were obtained using the single hot wire ($u'_{1,1}$), cross wire ($u'_{3,1}$) and a pair of single hot wires ($u'_{1,3}$). If the corrections were exact, the corrected derivatives would exhibit no dependence on the separation distance between the probes. In the centerline region of the wake the correction procedure works very well whereas in the outer part it underestimates expectations. This may be attributed to larger deviations from local isotropy in the outer part of the wake. Because the Kolomogorov length scale L_k increases with the distance from the wake centerline by a factor of about two, the relative separation between the sensors $\Delta x/L_k$ decreases and the poor performance of the corrections in

[3]For the plane case the values of L_k were 0.44 mm near the wake centerline ($\eta \simeq 0$) and 0.75 mm in the outer part ($\eta \simeq 2$) of the wake. The corresponding values for the axisymmetric case were 0.55 and 1.05 mm, respectively

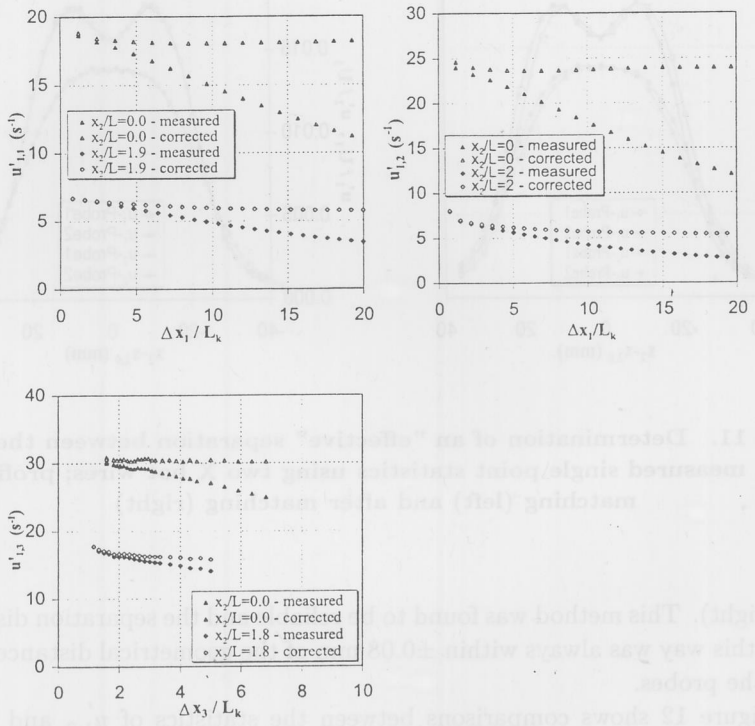

Figure 10. Measured and corrected statistics of the velocity derivatives $u'_{1,1}$, $u'_{3,1}$ and $u'_{1,3}$ at the centerline ($x_2/L \simeq 0$) and in the outer part ($x_2/L \simeq 1.8-2$) of the plane wake

the outer part of the wake is not so critical.

For very small separations between the probes, the influence of noise causes the derivatives to increase. Owing to the decreasing signal-to-noise ratio, this effect is noticeable in the outer part of the wake. An average separation between the probes of 1.7 mm corresponding to $\approx 4L_k$ near the centerline and $\approx 2L_k$ near the edge of the wake was found to be an optimal compromise between sufficient signal-to-noise ratio and a small amount of correction (3-5%) due to spatial averaging.

The separation between the individual X hot-wire probes was estimated from the average of the measured distances between the four pairs of supporting prongs. However, it was also possible to find an effective probe distance by shifting the statistics measured with hot-wire configurations shown in Fig. 1(a) and (d). Figure 11 (left) shows the measured profiles of the u'_1 and u'_2 intensities in the plane wake. By matching the measured profiles one obtains the effective probe distance as shown in

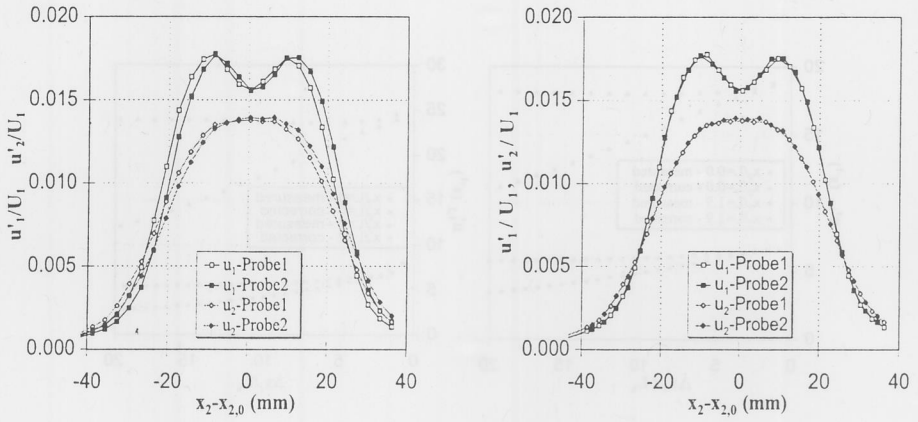

Figure 11. Determination of an "effective" separation between the probes from the measured single point statistics using two X hot wires; profiles before matching (left) and after matching (right)

Fig. 11 (right). This method was found to be reliable and the separation distance estimated in this way was always within ± 0.08 mm of the geometrical distance measured between the probes.

Figure 12 shows comparisons between the statistics of $u'_{1,2}$ and $u'_{1,3}$ using the probe configurations shown in Fig. 1 and the data obtained from a pair of two single hot wires. This figure also includes the statistics for $u'_{1,1}$ obtained by invoking Taylor's hypothesis. The displayed data were obtained in the axisymmetric wake and include profiles measured across both sides of the wake. The agreement achieved between various measurements of $u'_{1,1}$ is very good. A similar degree of agreement was obtained for $u'_{2,1}$ and $u'_{3,1}$ using different X hot-wire configurations (not shown). The agreement between the data for $u'_{1,2}$ and $u'_{1,3}$ measured using a pair of single hot wires and configurations (a) and (b) shown in Fig. 1 is also good. However, there is some discrepancy in the data measured with configuration (d) shown in Fig. 1. The same observations were made in the plane wake, with the exception that deviations of about 10% were obtained between the measured data for configurations (b) and (c). The origin of these deviations cannot be explained by spatial filtering effects due to the finite resolution of the hot wires employed. It might be associated with the phase differences between signals related to the separation between the wires which cannot be accouted for using the spectral corrections. In general, however, the accuracy can be considered to be satisfactory.

Figure 13 shows comparisons with the results from Browne *et al.* [14] and Ye [18]. Statistics of the streamwise derivatives from Ye [18] show qualitatively the same

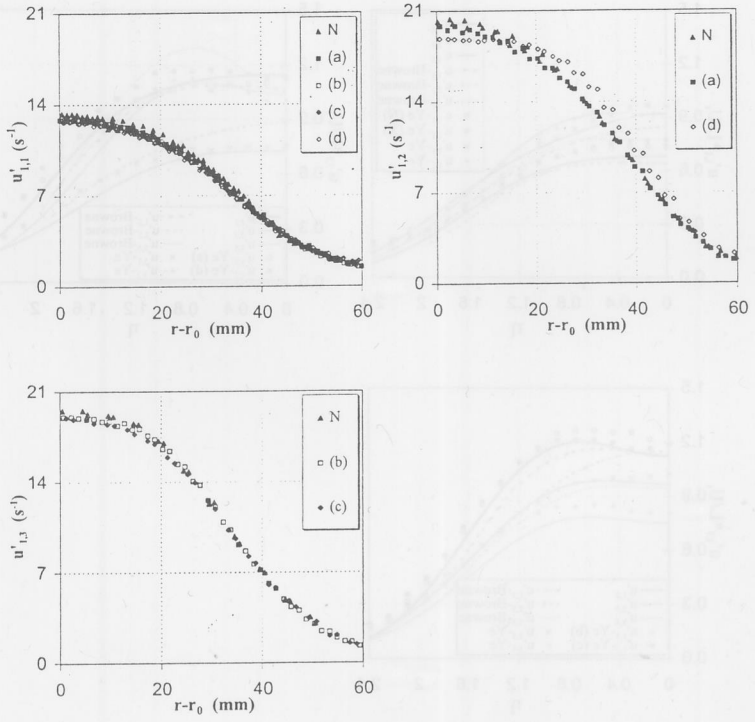

Figure 12. Comparisons of $u'_{1,1}$, $u'_{1,2}$ and $u'_{1,3}$ measured with hot-wire configurations (a), (b), (c) and (d) shown in Fig. 1 with measurements taken using a single wire and a pair of single hot wires (denoted N) in the axisymmetric wake

behavior but are 5-10% higher than the present values. The reason for this can be attributed to the electronic noise, since Ye [18] used a 3 dB filter and computed the derivatives directly from time series sampled at 10 kHz. Browne *et al.* [14] did not apply any corrections to the measured data that were sampled at a frequency of 5 kHz, which corresponds to $\Delta x_1/L_k \approx 3$. Measured statistics for the derivatives in the x_2 and x_3 directions are in good agreement with the data from Ye [18]. Deviations from the data measured by Ye are in the outer part of the wake and most probably originate from uncertainties in the position of the centerline, since she measured only half of the wake width. It must be mentioned, however, that Ye [18] did not correct her data for the finite length of the hot wires and probe and wire separation effects. The agreement of $u'_{1,2}$ and $u'_{1,3}$ with the data of Browne *et al.* [14] is good. The remaining statistics for the derivatives $u'_{2,2}$, $u'_{2,3}$, $u'_{3,2}$ and $u'_{3,3}$ show significant deviations. The reason for this

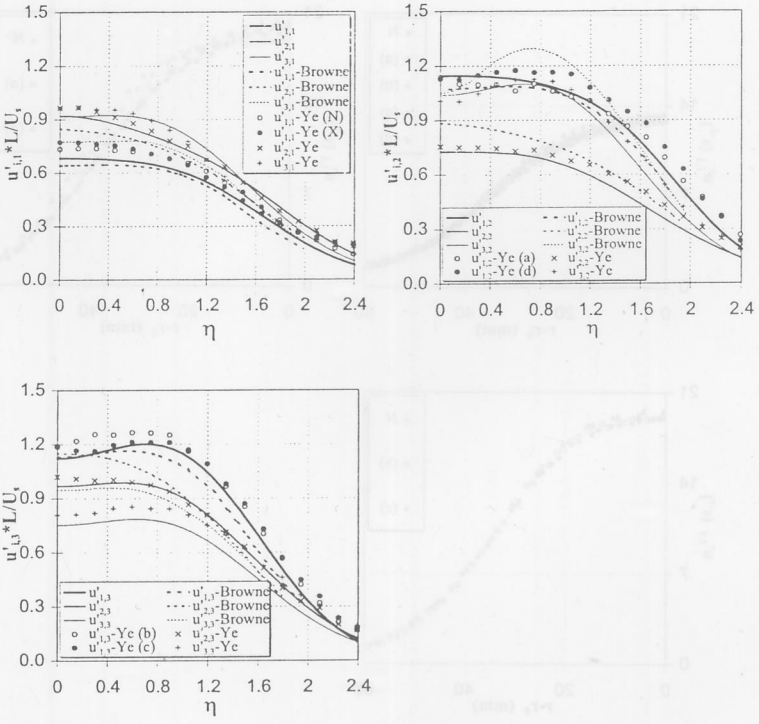

Figure 13. Comparisons of the statistics of all nine derivatives $u'_{i,j}$ in the plane wake with the data of Browne et al. [14] and Ye [18]

lies in the experimental difficulties associated with derivative measurements. In the next section we provide support for our measurements based on rational arguments.

Validation of the assumptions of local isotropy and local axisymmetry

The measured statistics of the velocity derivatives were used to check the assumptions of local isotropy and local axisymmetry. Local isotropy requires

$$\overline{\left(\frac{\partial u_i}{\partial x_k}\right)\left(\frac{\partial u_j}{\partial x_l}\right)} = \frac{1}{2}\overline{\left(\frac{\partial u_1}{\partial x_1}\right)^2}(4\delta_{ij}\delta_{kl} - \delta_{il}\delta_{jk} - \delta_{jl}\delta_{ik}) \tag{9}$$

from which it follows that in such a turbulence the ratios K_i must be equal to unity:

$$K_1 = \frac{2\overline{(\partial u_1/\partial x_1)^2}}{\overline{(\partial u_2/\partial x_1)^2}}, \quad K_2 = \frac{2\overline{(\partial u_1/\partial x_1)^2}}{\overline{(\partial u_3/\partial x_1)^2}}, \quad K_3 = \frac{2\overline{(\partial u_1/\partial x_1)^2}}{\overline{(\partial u_1/\partial x_2)^2}},$$

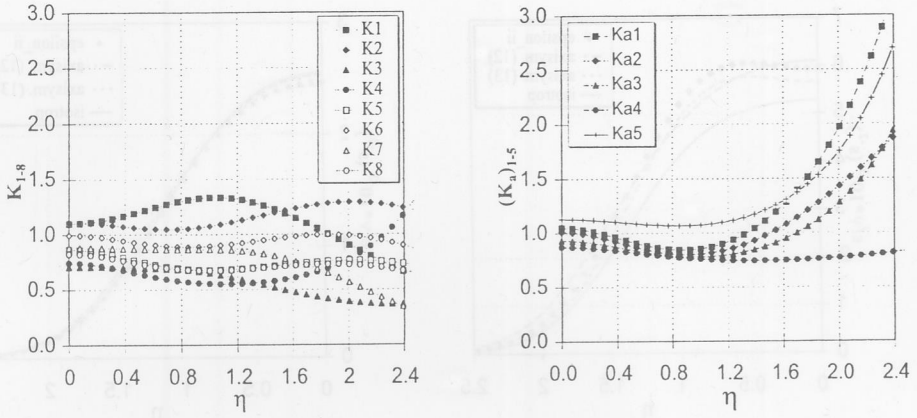

Figure 14. Distributions of the isotropic ratios $K_1 - K_8$ (left) and the axisymmetric ratios $K_{a1} - K_{a5}$ (right) across the plane wake

$$K_4 = \frac{2\overline{(\partial u_1/\partial x_1)^2}}{\overline{(\partial u_1/\partial x_3)^2}}, \quad K_5 = \frac{2\overline{(\partial u_1/\partial x_1)^2}}{\overline{(\partial u_3/\partial x_2)^2}}, \quad K_6 = \frac{2\overline{(\partial u_1/\partial x_1)^2}}{\overline{(\partial u_2/\partial x_3)^2}},$$

$$K_7 = \frac{\overline{(\partial u_1/\partial x_1)^2}}{\overline{(\partial u_2/\partial x_2)^2}}, \quad K_8 = \frac{\overline{(\partial u_1/\partial x_1)^2}}{\overline{(\partial u_3/\partial x_3)^2}} \tag{10}$$

In a similar way, one can derive the ratios K_{ai} for the case of locally axisymmetric turbulence (George and Hussein [15]):

$$K_{a_1} = \frac{\overline{(\partial u_1/\partial x_2)^2}}{\overline{(\partial u_1/\partial x_3)^2}}, \qquad K_{a_2} = \frac{\overline{(\partial u_2/\partial x_1)^2}}{\overline{(\partial u_3/\partial x_1)^2}}, \qquad K_{a_3} = \frac{\overline{(\partial u_2/\partial x_2)^2}}{\overline{(\partial u_3/\partial x_3)^2}},$$

$$K_{a_4} = \frac{\overline{(\partial u_2/\partial x_3)^2}}{\overline{(\partial u_3/\partial x_2)^2}}, \quad K_{a_5} = \frac{3\overline{(\partial u_2/\partial x_2)^2}}{\overline{(\partial u_1/\partial x_1)^2} + \overline{(\partial u_2/\partial x_3)^2}} \tag{11}$$

Figure 14 shows profiles of the individual ratios K_1-K_8 and K_{a1}-K_{a5} in the plane wake. According to the results reported in the literature, the deviations from local isotropy and local axisymmetry grow with increasing distance from the wake centerline. Our results show relatively small deviations from local isotropy near the wake centerline and are in agreement with measurements of Townsend [6] and Ye [18] but at variance with the results of Browne *et al.* [14]. Owing to moderate deviations from local isotropy, the isotropic estimate of the dissipation rate $\epsilon^{iso} = 15\nu\overline{(\partial u_1/\partial x_1)^2}$, shown in Fig. 15, is about 12% lower than the true value of ϵ at the wake centerline.

Figure 14 (right) suggests that local axisymmetry is a better approximation than local isotropy. In the inner part of the wake all ratios and $K_{a1} - K_{a5}$ are within

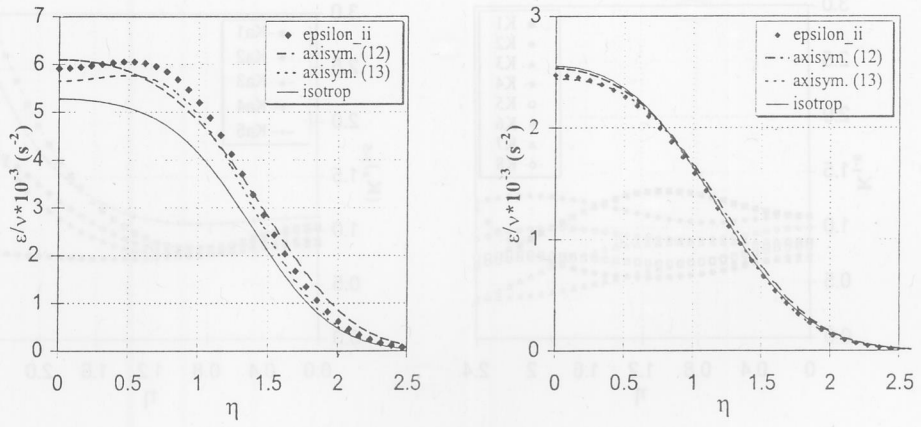

Figure 15. Comparison of the measured dissipation rate ϵ_{ii} with its isotropic and axisymmetric approximations in the plane (left) and axisymmetric (right) wake

experimental accuracy close to unity. In the outer part of the wake the deviations from local axisymmetry increase. Figure 14 (left) indicates that the axisymmetric estimates of ϵ, which may be defined in different ways owing to the identities (11) (Rotta, [34]):

$$\epsilon^{axi} = \nu \left[-\overline{(\partial u_1/\partial x_1)^2} + 2\overline{(\partial u_1/\partial x_2)^2} + 2\overline{(\partial u_2/\partial x_1)^2} + 8\overline{(\partial u_2/\partial x_2)^2} \right] \tag{12}$$

or

$$\epsilon^{axi} = \nu \left[\frac{5}{3}\overline{(\partial u_1/\partial x_1)^2} + 2\overline{(\partial u_1/\partial x_3)^2} + 2\overline{(\partial u_2/\partial x_1)^2} + \frac{8}{3}\overline{(\partial u_2/\partial x_3)^2} \right] \tag{13}$$

are in good agreement with the results of direct measurements.

The data for the axisymmetric wake are displayed in Fig. 16. Deviations from local isotropy and local axisymmetry in the centerline region of the wake are even smaller than in the plane case. Both isotropic and axisymmetric estimates for ϵ are in very good agreement with the true value of ϵ deduced from direct measurements of all nine terms involved in ϵ (see Fig. 15, right).

We may provide additional support for the results shown in Figs. 14-16 by exploring the results obtained from invariant theory. Using this theory, Jovanović and Otić [35] derived the exact relation between the anisotropies of the large and small scales in axisymmetric turbulence:

$$e_{ij} = \mathcal{A} a_{ij} \tag{14}$$

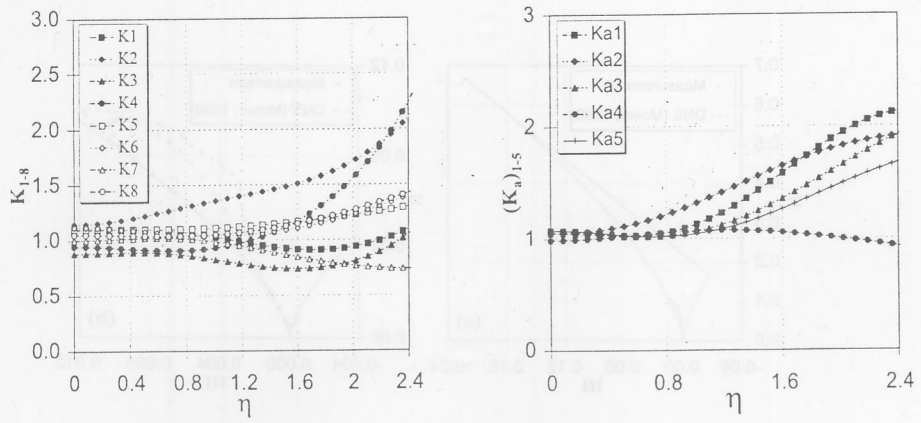

Figure 16. Distributions of the isotropic ratios $K_1 - K_8$ (left) and the axisymmetric ratios $K_{a1} - K_{a5}$ (right) across the axisymmetric wake

where a_{ij} and e_{ij} are defined as follows:

$$a_{ij} = \frac{\overline{u_i u_j}}{\overline{q^2}} - \frac{1}{3}\delta_{ij} \tag{15}$$

$$e_{ij} = \frac{\epsilon_{ij}}{\epsilon} - \frac{1}{3}\delta_{ij} \tag{16}$$

and $\mathcal{A}$ is a scalar function. Eq. (14) shows that anisotropy of turbulence in the dissipation range is directly proportional to the anisotropy of turbulence at large scales. To quantify anisotropy, Lumley [36] introduced scalar invarants of a_{ij}:

$$\mathrm{II} = a_{ij}a_{ji} \tag{17}$$

$$\mathrm{III} = a_{ij}a_{jk}a_{ki} \tag{18}$$

to show that these can be interrelated analytically for two-component turbulence:

$$\mathrm{II} = 2/9 + 2\mathrm{III} \tag{19}$$

and axisymmetric turbulence:

$$\mathrm{II} = (2/3)[(4/3)|\mathrm{III}|]^{2/3} \tag{20}$$

The cross-plot of II versus III constructed from eqs. (19) and (20) defines the anisotropy invariant map which bounds all physically realizable turbulence.

By plotting the experimental data on the anisotropy invariant map (Fig. 17), one can clearly observe that, in the inner part of the wake behind the sphere, turbulence is almost exactly axisymmetric. Also, the data of the plane wake show only

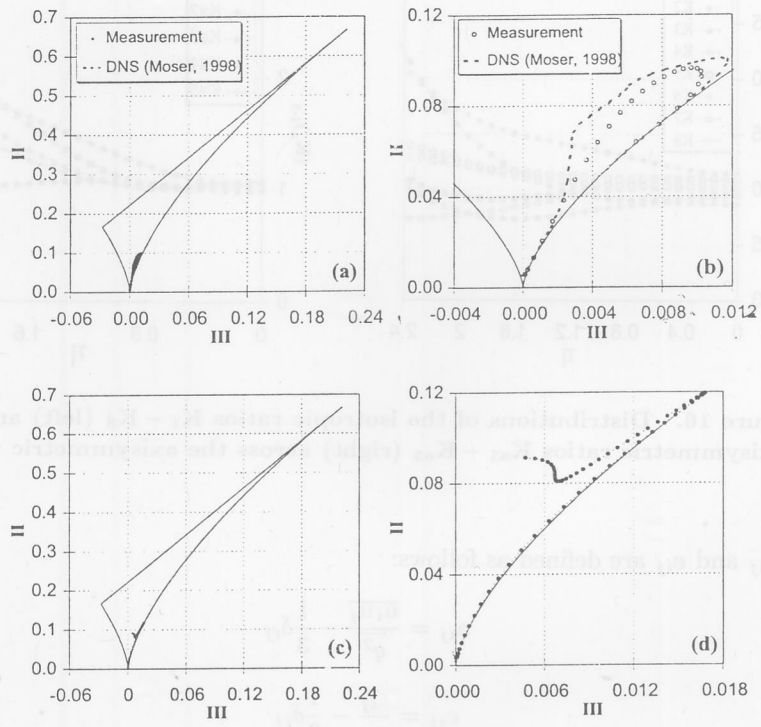

Figure 17. Traces of joint variations of the invariants across the plane wake (top, left-right) and the axisymmetric wake (bottom, left-right) within the anisotropy-invariant map

moderate deviations from the axisymmetric state. Figure 17 shows that these results are supported by the DNS data of Moser *et al.* [37], who performed direct numerical simulations of the plane wake flow. Taking these results into account, it follows from eq. (14) that the anisotropy at small scales and therefore of ϵ_{ij} must vanish near the wake centerline.

The balance of the energy equation

The experimental data were used to compute the budget of the turbulent kinetic energy $k = \overline{u_k u_k}/2 = \overline{q^2}/2$. For the two-dimensional wake flow the transport

equation for k is

$$\underbrace{U_1 \frac{\partial}{\partial x_1}\frac{\overline{q^2}}{2}}_{\text{Convection}} = \underbrace{-\overline{u_1 u_2}\frac{\partial U_1}{\partial x_2}}_{\text{Production}} \underbrace{-\frac{1}{2}\frac{\partial}{\partial x_2}\overline{q^2 u_2}}_{\overline{q^2}-\text{Diffusion}} \underbrace{-\frac{1}{\rho}\frac{\partial}{\partial x_2}\overline{pu_2}}_{\text{Pressure-Diffusion}} - \underbrace{\epsilon}_{\text{Dissipation}} \tag{21}$$

The viscous diffusion was neglected in eq. (21) since it was found to be much smaller than the other terms involved in the budget of k.

The convection term was estimated from the self-similarity of the profiles, $\overline{q^2}/U_S^2 = \tilde{\overline{q^2}}(\eta)$. Production and diffusion terms were computed directly from the measured profiles of the mean velocity, shear stress and triple moments. The pressure diffusion was deduced from the balance of eq. (21) by difference.

The distributions of all terms involved in the balance of eq. (21), normalized by L/U_S^3, are shown in Fig. 18 (left). At the wake centerline convection and turbulent diffusion are balanced by the dissipation. The pressure-diffusion is small compared with the other terms. A similar observation was made by Ye [18] and Browne *et al.* [14]. The integral constraints for the diffusion terms

$$\int_0^\infty \frac{\partial}{\partial \eta}(\overline{q^2 u_2})d\eta = 0 \quad \text{and} \quad \int_0^\infty \frac{\partial}{\partial \eta}(\overline{pu_2})d\eta = 0 \tag{22}$$

were satisfied within 1.5% and 15%, respectively, relative to the absolute value of the corresponding integral. One should note that the pressure-diffusion is small compared with the turbulent diffusion and therefore is strongly influenced by small measuring errors of the terms dominating the balance of k. For example, the integral of the pressure-diffusion term tends to zero if the dissipation rate is underestimated by 2%.

The DNS data of Moser *et al.* [37], which are plotted in Fig. 18 (right), show nearly the same trends in the behavior of the individual terms of the energy balance (21) as our experimental results. One should note that Moser *et al.* [37] simulated the time-developing wake whereas our experimental investigations correspond to the spatially developing wake.

For the axisymmetric wake the energy equation is

$$\underbrace{U_1 \frac{\partial}{\partial x_1}\frac{\overline{q^2}}{2}}_{\text{Convection}} = \underbrace{-\overline{u_1 u_2}\frac{\partial U_1}{\partial r}}_{\text{Production}} \underbrace{-\frac{1}{2r}\frac{\partial}{\partial r}r\overline{q^2 u_2}}_{\overline{q^2}-\text{Diffusion}} \underbrace{-\frac{1}{\rho}\frac{1}{r}\frac{\partial}{\partial r}r\overline{pu_2}}_{\text{Pressure-Diffusion}} - \underbrace{\epsilon}_{\text{Dissipation}} \tag{23}$$

Figure 19 shows the distributions of the individual terms involved in eq. (23), normalized by L/U_S^3. The production of k is seen to be much smaller than in the plane case. This observation and the whole energy balance is in very good agreement with the data of Uberoi and Freymuth [38]. It should be mentioned, however, that they computed the diffusion terms directly from the balance of eq. (23) and found

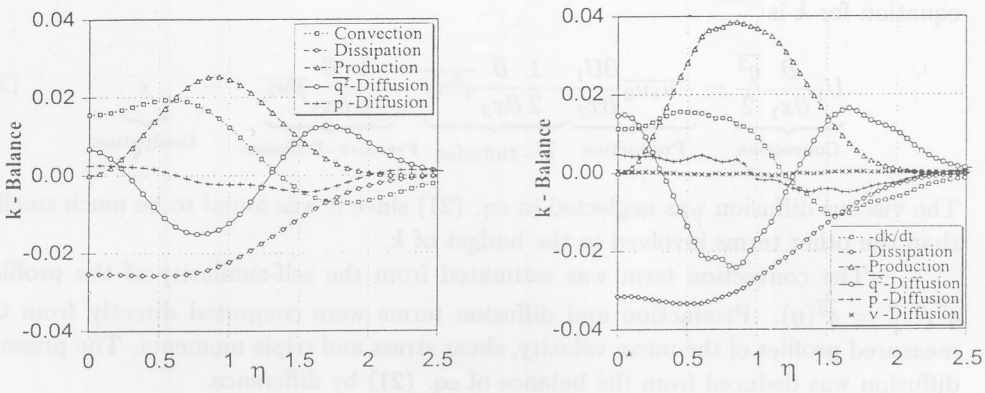

Figure 18. Budget of the turbulent kinetic energy in the plane wake: measurements (left); DNS of Moser et al. [37] (right)

that these do not satisfy the integral constraints. An explanation for this might lie in the uncertainty of the estimated convection term. We encountered a similar problem and therefore decided to estimate the convection term directly by computing the streamwise derivative from the measured longitudinal intensity component assuming that the changes of the anisotropy in the streamwise direction are negligible. The turbulent and pressure diffusion which were obtained by difference from eq. (23) satisfy the integral constraints within 1.5% and 6%, respectively. Figure 19 implies that in the axisymmetric wake the pressure diffusion cannot be neglected and follows qualitatively the suggestion made by Lumley [36], $\overline{u_i p}/\rho \approx -0.2\overline{q^2 u_i}$.

CONCLUSION

Measurements of all first-order spatial derivatives of the instantaneous velocity fluctuations in plane and axisymmetric small-deficit turbulent wakes were performed using a pair of X wires. Errors due to finite length of the hot wires and due to the wire and probe spacing effects were analyzed and accounted for in evaluation of the data.

The experimental results were systematically checked and were found to be consistent with the dynamic equations for the turbulence quantities and also with the data available in the literature. The assumptions of local isotropy and local axisymmetry were examined. Both investigated wake flows deviate only moderately from local isotropy and local axisymmetry.

The assumption of local axisymmetry was found to be a better approximation than the assumption of local isotropy. The axisymmetric estimate of the turbulent dissipation rate was found to be a good approximation for both plane and axisymmet-

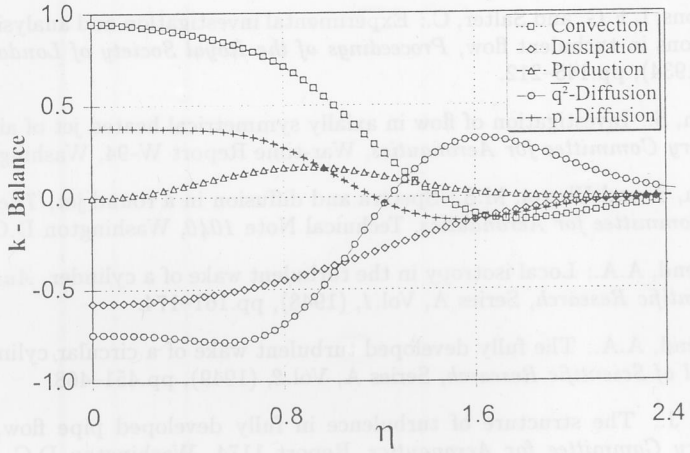

Figure 19. Budget of the turbulent kinetic energy in the axisymmetric wake

ric wake flows. The results presented demonstrate that the isotropic approximation of the dissipation rate underestimates the true value of ϵ between 10% near the wake centerline and 25% in the outer part of the plane wake. In the case of the axisymmetric wake the isotropic dissipation computed by assuming local isotropy gives an excellent estimate in comparison with direct measurements.

The budget of the turbulent kinetic energy was computed from the data. The individual terms of the k equation show the plausible distributions with the diffusion terms which satisfy the integral constraints. While the pressure transport is nearly negligible in the plane wake, it plays an important role in the axisymmetric wake and follows closely Lumley's [36] suggestion, $\overline{u_i p}/\rho \approx -0.2\overline{q^2 u_i}$.

ACKNOWLEDGEMENTS

This research received financial support in part from the Volkswagen-Stiftung within the project "Development of statistical models of turbulence using the experimental and numerical databases" (I/72 857) and by the Deutsche Forschungsgemeinschaft (Grant Jo 240/1-3).

REFERENCES

[1] Kolmogorov, A.N.: Local structure of turbulence in an incompressible fluid at very high Reynolds numbers, *Comptes Rendus (Doklady) de l'Académie des Sciences de l'U.R.S.S.*, Vol.*30*, (1941), pp.299–303.

[2] Simmons, L.F.G. and Salter, C.: Experimental investigation and analysis of the velocity variations in turbulent flow, *Proceedings of the Royal Society of London,* Sries A, Vol. *165*, (1934), pp.145–212.

[3] Corrsin, S.: Investigation of flow in axially symmetrical heated jet of air, *The National Advisory Committee for Aeronautics*, War-time Report W-94, Washington D.C., 1943.

[4] Corrsin, S. and Uberoi, M.S.: Spectra and diffusion in a round jet, *The National Advisory Committee for Aeronautics*, Technical Note *1040*, Washington D.C., 1951.

[5] Townsend, A.A.: Local isotropy in the turbulent wake of a cylinder, *Australian Journal of Scientific Research,* Series A, Vol.*1*, (1948), pp.161–174.

[6] Townsend, A.A.: The fully developed turbulent wake of a circular cylinder, *Australian Journal of Scientific Research,* Series A, Vol.*2*, (1949), pp.451–468.

[7] Laufer, J.: The structure of turbulence in fully developed pipe flow, *The National Advisory Committee for Aeronautics*, Report 1174, Washington D.C., 1954, pp.417–433.

[8] Klebanoff, J.: Characteristics of turbulence in a boundary layer with zero pressure gradient, *The National Advisory Committee for Aeronautics*, Technical Note 3178, Washington D.C., 1953.

[9] Uberoi, M.S. and Freymuth, P.: Temperature fluctuations in the turbulent wake behind an optically heated sphere, *Physics of Fluids*, Vo.*16*, (1973), pp.161–168.

[10] Antonia, R.A. and Browne, L.W.B.: Anisotropy of the temperature dissipation in a turbulent wake, *Journal of Fluid Mechanics*, Vol.*163*, (1986), pp.393–403.

[11] Tavoularis, S. and Corrsin, S.: Experiments in nearly homogeneous turbulent shear flow with uniform mean temperature gradient. Part 1, *Journal of Fluid Mechanics*, Vol.*104*, (1981), pp.311–347.

[12] Tavoularis, S. and Corrsin, S.: Experiments in nearly homogeneous turbulent shear flow with uniform mean temperature gradient. Part 2, *Journal of Fluid Mechanics*, Vol.*104*, (1981), pp.349–367.

[13] Krishnamoorthy, L.V. and Antonia, R.A.: Temperature-dissipation measurements in a turbulent boundary layer, *Journal of Fluid Mechanics*, Vol.*176*, (1987), pp.265–281.

[14] Browne, L.W.B., Antonia, R.A. and Shah, D.A.: Turbulent energy dissipation in a wake, *Journal of Fluid Mechanics*, Vol.*179*, (1987), pp.307–326.

[15] George, W.K. and Hussein, H.J.: Locally axisymmetric turbulence, *Journal of Fluid Mechanics*, Vol.*233*, (1991), pp.1–23.

[16] Hussein, H.J., Capp, S.P. and George, W.: Velocity measurements in a high Reynolds number, momentum-conserving, axisymmetric, turbulent jet, *Journal of Fluid Mechanics*, Vol.*258*, (1994), pp.31–75.

[17] Hussein, H.J.: Evidence of local axisymmetry in the small scales of a turbulent planar jet, *Physics of Fluids*, Vol.*6*, (1994), pp.2058–2070.

[18] Ye, Q.-Y.: Die turbulente Dissipation mechanischer Energie in Scherschichten, Dissertation, Universität Erlangen-Nürnberg, 1996.

[19] Zhu, Y. and Antonia, R.A.: The spatial resolution of hot-wire arrays for the measurement of small-scale turbulence, *Measurement Science and Technology*, Vol.*7*, (1996), pp.1349–1359.

[20] Wyngaard, J.C.: Measurement of small-scale turbulence structure with hot wires, *Journal of Scientific Instruments*, Vol.*1*, (1968), pp.1105–1108.

[21] Wyngaard, J.C.: Spatial resolution of the vorticity meter and other hot-wire arrays, *Journal of Scientific Instruments*, Vol.*2*, (1969), pp.983–987.

[22] Pao, Y.-H.: Structure of turbulent velocity and scalar fields in large wave numbers, *Physics of Fluids*, Vol.**8**, (1965), pp.1063–1075.

[23] Schenck, T.C.: Messung der turbulenten Dissipationsrate in ebenen und achsensymmetrischen Nachlaufströmungen, Dissertation, Universität Erlangen-Nürnberg, 1999.

[24] Bradshaw, P.: *An Introduction to Turbulence and its Measurement*, Pergamon Press, Oxford, 1971.

[25] Wygnanski, I. and Fiedler, H.: Some measurements in the self-preserving jet, *Journal of Fluid Mechanics*, Vol.*38*, (1969), pp.577–612.

[26] Kaiser, J.F., and Reed, W.A.: Data smoothing using low-pass digital filters, *Review of Scientific Instruments*, Vol.*48*, (1977), pp.1447–1457.

[27] Wygnanski, I., Champagne, F. and Marasli, B.: On the large-scale structures in two-dimensional, small-deficit, turbulent wake, *Journal of Fluid Mechanics*, Vol.*168*, (1986), pp.31-71.

[28] Hoerner, S.F.: *Fluid-Dynamic Drag*, Hoerner Fluid Dynamics, P.O. Box 342, Brick Town, N.J. 08723, 1965.

[29] Schlichting, H. and Gersten, K.: *Grenzschicht-Theorie*, Springer-Verlag, Berlin, Heidelberg, 1997.

[30] Fabris, G.: Third-order conditional transport correlations in the two-dimensional turbulent wake, *Physics of Fluids*, Vol.*26*, (1983), pp.422–427.

[31] Aronson, D. and Löfdahl, L.: The plane wake of a cylinder: measurements and inferences on turbulence modeling, *Physics of Fluids*, Vol.*5*, (1993), pp.1433–1437.

[32] Uberoi, M.S. and Freymuth, P.: Spectra of turbulence in wakes behind circular cylinders, *Physics of Fluids*, Vol.*12*, (1969), pp.1359–1363.

[33] George, W.K.: The self-preservation of turbulent flows and its relation to initial conditions and coherent structures, In *Advances in Turbulence* (ed. W.K. George & R. Arndt), Hemisphere, 1989, pp.39-73.

[34] Rotta, J.C.: *Turbulente Strömungen*, B.G.Taubner, Stuttgart, 1972.

[35] Jovanović J., and Otić I.: On the constitutive relation for the Reynolds stresses and the Prandtl-Kolmogorov hypothesis of effective viscosity in axisymmetric strained turbulence, *Journal of Fluids Engineering*, Vol.*122*, (2000), pp.48–50.

[36] Lumley, J.: Computational modeling of turbulent flows, *Advances in Applied Mechanics*, Vol.*18*, (1978), pp.123–176.

[37] Moser, R.D., Rogers, M.M. and Ewing, D.W.: Self-similarity of time-evolving plane wakes, *Journal of Fluid Mechanics*, Vol.*367*, (1998), pp.255–289.

[38] Uberoi, M.S. and Freymuth, P.: Turbulent energy balance and spectra of the axisymmetric wake, *Physics of Fluids*, Vol.*13*, (1970), pp.2205–2210.

Authors address:

T. C. Schenck, J. R. Jovanović
Institute of Fluid Mechanics
University Erlangen-Nürnberg
Cauerstraße 4, D–91058 Erlangen
Germany

Paper submitted: November 30, 2001
Paper revised: February 26, 2002
Paper accepted: March, 18 2002